Mechanical behaviour of tape springs used in the deployment of reflectors around a solar panel

Florence Dewalque[1], Jean-Paul Collette[2], Olivier Brüls[1]

[1]Department of Aerospace and Mechanical Engineering, University of Liège, Belgium
[2]Walopt, Embourg, Belgium

Abstract

In order to increase the production of power on small satellites, solar panels are commonly deployed and, in some cases, reflectors are added to improve the concentration factor on solar cells. In this work, reflectors are deployed by the means of compliant mechanisms known as tape springs. Their attractive characteristics are, among others, their passive behaviour, their self-locking capacity, their elastic deformations and their robustness. However, their mechanical behaviour is highly nonlinear and requires thorough analyses in order to develop predictive numerical models. It is shown here through parametric studies that the nonlinear behaviour of a tape spring is mainly governed by its geometry. Thus, for each specific application, its dimensions can be determined in order to minimise two critical features: the maximum stress affecting the structure and the maximum motion amplitude during deployment. In this paper, an optimisation procedure is proposed to meet these requirements.

Keywords: tape springs, nonlinear behaviour, shells, compliant deployable structure, reflectors, optimisation

1 Introduction

In deployable structures, various types of mechanisms can be used to connect the different bodies. The most common ones are usually composed of kinematic joints and have to be combined with a motor to perform the deployment stage. Nonetheless, compliant systems have been developed and proved reliable in various engineering applications [1]. In this present work, the inherent characteristics of tape springs, belonging to this last category, are exploited in a space application.

By definition, some elastic energy is stored during their folding and is then naturally released during deployment in order to reach an equilibrium configuration. Although two equilibrium states may exist [1], only the straight one is sought in the following studied cases. The deployment stage is thus completely passive and self-actuated, requiring no external source of energy as opposed to the most common joints. Compared to these latter, other significant advantages can be pointed out. No lubricant is needed since the motion results from the deformation of structural components only and not from the sliding between contact surfaces. Thus, the risks of outgassing and contamination are reduced in space environment. The structural simplicity of tape springs is also a strong asset since it greatly improves the robustness and limits the possibilities of failure during folding and deployment.

The complexity of tape springs comes from their highly nonlinear mechanical behaviour. First of all, according to the sense of bending, different deformed configurations are encountered.

For example, the equal sense is characterised by some torsion, while in the opposite sense, the structure is not affected by any transverse displacements. Then, for a critical value of the rotation angle, the tape spring is submitted to buckling which induces the formation of a fold and a sudden drop in the stiffness. Finally, due to the non-superposition of the loading and unloading paths, the dynamic evolution is affected by some hysteresis which, after a certain number of cycles, leads to the self-locking of the structure.

Wüst [2], Rimrott [3] and Mansfield [4] derived the theoretical relationship between the applied rotation angle and the associated bending moment. Various analytical models were developed: in [5], tape springs are represented as two rigid bodies of variable length interconnected by a mobile hinge; in [6], a variational approach expressed in terms of potential energy is used to perform quasi-static analyses; in [7, 8], a one-dimensional planar rod model with a flexible cross-section is investigated. Numerous finite element analyses exploiting shells were also achieved. For example, static analyses of a large variety of tape springs can be found in [9], while dynamic analyses focusing on the self-locking phenomenon, on the impact of the numerical and structural dampings, and on three-dimensional tape springs are available in [10], [11] and [12] respectively. Finally, experimental studies were performed to either validate analytical or finite element analyses. Static and dynamic tests can be found in [5, 13] and [5, 14, 15] respectively.

The choice of the application studied in this paper was made by taking into consideration the growing interest in the development of technologies for small satellites of less than 200 kg. The intended purpose is the launch of numerous missions requiring both a low budget and a short period of design. Regarding the on-board power consumption of the electronic equipment, it is generally not possible or enough to cover the external surface of the satellite with solar cells. The most common solution is then to deploy solar panels on the sides of the satellite once it is jettisoned from the rocket. Furthermore, adding reflectors along the solar panels concentrates the sunlight on the solar cells and thus, in theory, the geometric concentrator factor can be doubled and the area of the solar panels can be reduced. This system, however, requires the folding of the panels and the reflectors in order to integrate the satellite inside the confined space of the fairing, hence the use of tape springs.

For space systems, the use of reflectors has been investigated since the nineties [16]. The V-trough concentrators were first integrated on the solar panels of the PanAmSat Galaxy XI satellite and, a few years later, they were exploited on the Boeing BSS-702 Satellite Bus with limited success due to the contamination of the reflecting surfaces and the shrinkage of the reflectors alignment system [17]. More recently, JAXA launched the small spacecraft REIMEI equipped with single lateral reflectors on each solar panel (Fig. 1) which gave satisfactory results according to their last report [18].

The use of reflectors is then not unusual to increase the performance of solar panels and deploying them with tape springs shows promising advantages. A particular deployment procedure exploiting the self-actuated and the self-locking properties of tape springs can be found in [19] where they provide the driving torques to classical hinges. In the present work, however, the hinges connecting the reflectors to the solar panels are only composed of tape springs and not combined to any additional classical hinges.

An extensive analysis is then required to prove their efficiency for this type of applications. During folding and then deployment, the most critical parameters are the maximum stresses affecting the structure and the maximum motion amplitude. Regarding the former, its value must be kept under the yield limit in order to remain in the elastic regime and prevent irreversible deformations, while for the latter, which is only relevant during deployment, any collision with the other elements of the spacecraft must be avoided. To fulfil these requirements, the geometry of the tape springs has to be adapted to each specific situation. Since several parameters can be modified, it is proposed in this work to address this problem by the means of an optimisation procedure exploiting the results of finite element models.

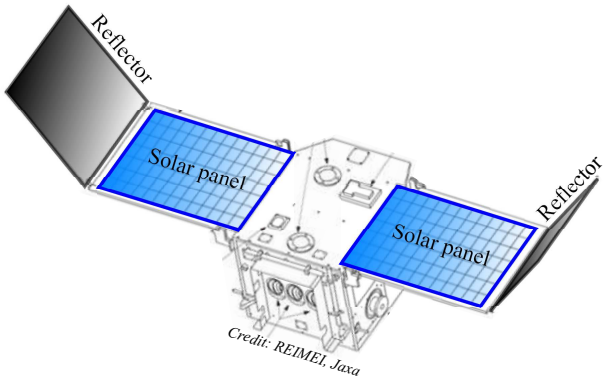

Figure 1: Deployed configuration of the reflectors on the spacecraft REIMEI (modified illustration from [18]).

The layout of this paper is as follows. In Section 2, the problem to be solved is defined, along with the geometric characteristics and the material properties of the tape springs. Then, in Section 3, their theoretical behaviour is recalled. In Section 4, the features of the finite element analyses and models are described. In Section 5, parametric studies are performed by varying some geometric parameters. The impact of the thickness and the radius of curvature are assessed. In Section 6, the optimisation procedure is performed to minimise the stresses and the motion amplitudes, while the complete deployment of the reflector will be discussed in Section 7. Finally, the conclusions of this work are drawn in Section 8.

2 Definition of the problem

The problem studied in this work is the deployment of a reflector around a fixed solar panel. In its folded configuration, it is located on the top of the panel. The reflective membrane is square of side 200 mm and, with its frame, has a mass of 0.4 kg. In its deployed configuration, the angle formed with the solar panel reaches 120° as recommended in [19]. The hinge is composed of two tape springs, whose orientation will be determined in the last part of this study.

The geometry of a tape spring is completely characterised by four parameters: its length L, its thickness t, its subtended angle α and its transverse radius of curvature R. Regarding the reference frame used in this work, the x-axis coincides with the longitudinal axis of the tape spring, the y-axis with its transverse axis and the z-axis is along the height. All these elements are represented in Fig. 2. Furthermore, only straight tape springs, that is without any initial longitudinal curvature, are considered in this paper. However, applications with curved tape springs can be found in [14].

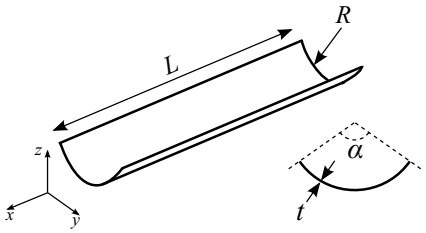

Figure 2: Geometric characteristics of a tape spring with the length L, the thickness t, the subtended angle α and the transverse radius of curvature R.

E	ν	ρ	σ_y
131000 MPa	0.3	8100 kg/m^3	1175 MPa

Table 1: Material properties of beryllium copper (source [9]).

In a spacecraft the available space is strictly limited and the one devoted to the hinges of the reflectors is most likely to be determined at an early stage of the spacecraft design. Here, the tape springs length is fixed to 50 mm, while for their cross-section, their width $w = 2R\sin\alpha/2$ and their height $h = R(1-\cos\alpha/2)$ cannot exceed 25 mm and 10 mm respectively. A schematic representation of the deployed reflector is given in Fig. 3, along with the maximum dimensions accepted for the tape springs. Notice that in order to simplify the model, all the connections between the different components (tape springs – solar panel, tape springs – reflector) will be considered as perfectly rigid.

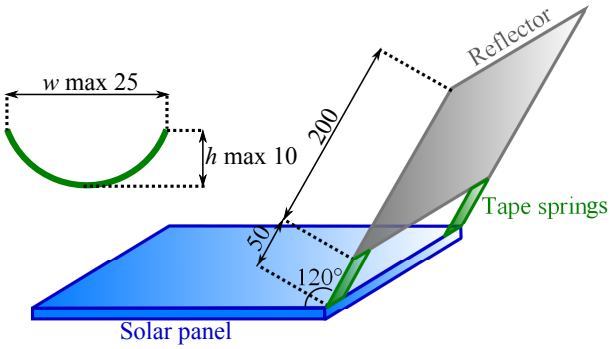

Figure 3: Deployed configuration of the reflector and maximum dimensions (in millimetres) of the tape springs.

Throughout the simulations, the thickness t, the radius of curvature R and the subtended angle α are the remaining design variables. Regarding the material composing the tape springs, its properties are fixed *a priori* in order to limit the complexity of the design problem in these first analyses, furthermore in space applications, the choice of materials is anyway limited due to constraining requirements on contamination. The chosen material used throughout this work is the beryllium copper. Its properties are given in Table 1 where E is the Young's modulus, ν the Poisson's ratio, ρ the density and σ_y the yield limit.

Finally, the objective functions to be minimised using the optimisation procedure are the maximum Von Mises stress and/or the maximum motion amplitude.

3 Quasi-static nonlinear behaviour of tape springs

Regarding the nonlinear behaviour of tape springs, the first characteristic feature clearly noticeable is the dependency of the deformed configuration to the sense of bending. These two senses and the corresponding sign convention defined by Wüst [2] are illustrated in Fig. 4. In the first case, the deformed structure is characterised by longitudinal and transverse curvatures in opposite sense, hence named opposite sense bending. The bending moment M and the bending angle θ are by definition positive. In the second case, the longitudinal and the transverse curvatures are in equal sense, hence named equal sense bending. Accordingly, the bending moment M and the associated bending angle θ are negative.

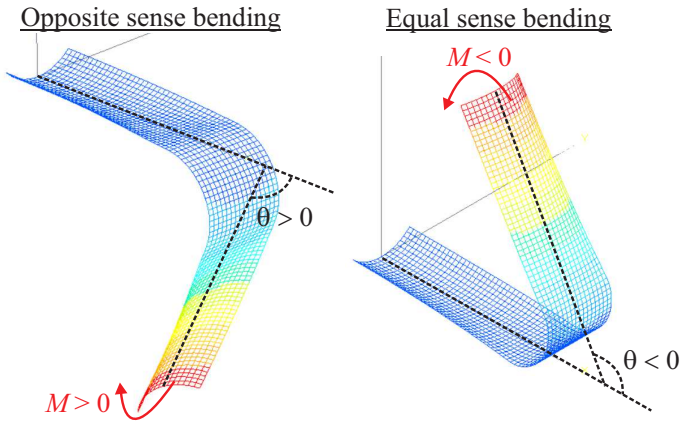

Figure 4: Illustration of the senses of bending and sign convention.

The theoretical behaviour of tape springs is defined based on the evolution of the bending moment M at the clamped extremity of the structure when the bending angle θ is controlled at the other end. The commonly acknowledged evolution for a quasi-static analysis is given in Fig. 5 (inspired from [9]). Comprehensive descriptions can be found in [5, 9, 14], while a simplified diagram is available in [20]. The major features are recalled here.

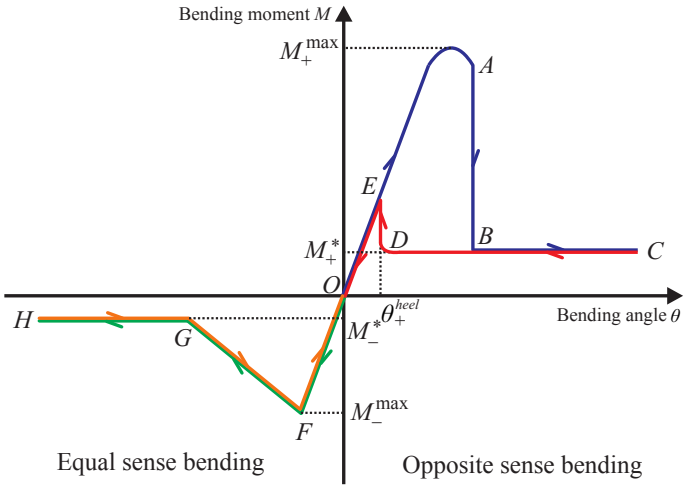

Figure 5: Theoretical evolution of the bending moment with the applied bending angle. Blue ($OABC$): loading in opposite sense; red ($CDEO$): unloading in opposite sense; green ($OFGH$): loading in equal sense; orange ($HGFO$): unloading in equal sense.

In opposite sense bending, starting from point O, the evolution of the bending moment M is linear for small rotation angles. The corresponding deformed configuration is characterised by a smooth curvature along the longitudinal axis. As the angle of rotation increases, the region located at the middle of the tape spring flattens until the associated bending moment reaches a maximum $M_+^{\max}$ called peak moment. Shortly after, the moment undergoes a dramatic drop (AB) which is due to the buckling of the structure leading to the formation of a fold. In this configuration, only the middle part of the tape spring is deformed due to the fold, while the rest of the structure remains straight (Fig. 4). Regarding the radius of curvature of the fold, it can be considered as a first approximation as equal to the transverse radius of curvature of the non-

deformed structure [2, 21]. However, finite element analyses showed that a difference exists [22], although marginal. Once buckling occurred, larger rotation angles induce in theory no change in the bending moment (BC) which is defined as the steady-state moment M_+^*. Regarding the deformed configuration, only the arc-length of the fold is affected by the variations of the bending angle. All this description is representative of the quasi-static loading or folding of a tape spring.

Regarding the controlled unloading of this loaded configuration, the first part of the curve (CB) is superimposed with the loading path. However, at point B, the red curve remains equal to M_+^* until point D is reached before jumping back on the loading curve at point E which corresponds to a deformed configuration without any fold. For the last part (EO), a linear evolution is recovered.

The fact that the fold does not disappear at the same angle of rotation as the one at which it is formed is responsible for some dissipation as cycles of loading–unloading are performed. This hysteresis phenomenon will, in the end, lead to the self-locking of the structure in its straight configuration.

In the equal sense bending, starting again from O, the relationship between the bending moment and the rotation angle rotation is linear (OF) and characterised by the same stiffness as in opposite sense. The peak moment is reached for a relatively small angle which implies that $|M_-^{\max}| < |M_+^{\max}|$. It is directly followed by buckling which, in this case, is due to asymmetric torsional folds converging from the extremities of the tape spring to its middle where they combine to form a symmetric fold. Then, as in opposite sense, the behaviour after buckling (GH) is defined by a constant steady-state moment M_-^*. Finally, it is commonly accepted that, in theory, the unloading path in equal sense coincides with the folding sequence, although in practice the adequacy is not perfect.

4 Finite element analyses

In the present work, all the finite element analyses are performed by the means of the commercial software Samcef [23]. Finite element shells are selected since the geometry of a tape spring is such that its thickness is several orders of magnitude smaller than all the other dimensions. Their behaviour is based on the Mindlin–Reissner theory which takes into account the shear deformations and elements with linear shape functions are chosen here. Indeed, tests were performed with quadratic shells, however, no significant modification on the results was noticed and it unnecessarily increased the computational cost.

The resolution of the problem is performed in two steps. Starting from the straight undeformed configuration, the tape spring is first folded until the rotation angle reaches the required value that represents the initial folded state of the structure. In this application, it corresponds to the reflector on top of the solar panel, that is an angle of 120°. This stage could be based on a static analysis, however, the associated continuation methods are quite sensitive and the determination of their numerical parameters cumbersome. In order to facilitate the folding analysis, a very slow dynamic analysis is preferred. As it was shown in [10], this choice has no significant impact on the results, except at the buckling instant where some numerical oscillations may appear in the solution. For that purpose, the bending velocity is constant and fixed to half a degree per second. The solver exploited at this quasi-static stage is the damped Newmark method [24] with first-order accuracy. The numerical damping parameters are chosen such that the corresponding spectral radius at infinite frequencies is equal to zero. Thus, the numerical damping is very high and the oscillations after buckling can be annihilated in a minimum number of time steps.

Once the tape spring reaches its folded configuration, the rotation constraint is released and the deployment is simulated without any external loads affecting the structure. In this

case, a classical dynamic analysis is implemented and the simulation is carried out until the oscillations are damped out and the structure reaches its fully deployed configuration. For more accuracy, the second-order time integration algorithm defined by the generalised-α method [25] is chosen.

For both solvers, an adaptive procedure is used to determine the time step. Thus, the nonlinear phenomena such as buckling, where small time steps are expected, can easily be captured, while the computational cost can be reduced when the evolution of the deformed structure is not significant by the means of a larger time step, whose maximum value is fixed by the operator.

In order to ensure the validity of the finite element results, convergence analyses were performed both in terms of space (convergence of the results when the mesh size decreases) and time (convergence of the results when the maximum time step decreases). It led to the choices of the mesh sizes and maximum time steps used in the following sections of this paper.

Regarding the geometry of the model, besides the parameters described in Section 2, two nodes coinciding with the centroids of the cross-sections at the extremities are added for the definition of the boundary conditions. They are rigidly connected to these cross-sections in order to facilitate the control of the bending angle and the acquisition of the results. The boundary conditions correspond to a clamp at one extremity and an imposed or free rotation angle at the other one for the folding and the deployment of the tape springs respectively. To represent the reflector, a lumped mass is located at its centre of mass and rigidly connected to the tape springs.

5 Parametric studies

Before starting an optimisation procedure involving several design variables, the impact of each one of them on the tape spring behaviour is assessed. Quasi-static analyses are performed on a tape spring of length 150 mm and made of beryllium copper (Table 1) which is bended up to an angle of 60° (resp. $-60°$) in opposite sense (resp. in equal sense), then, while still controlling the rotation angle, the structure is brought back to its straight configuration. Thus, the pair of curves (loading and unloading paths) schematically given in Fig. 5 are obtained. In order to have precise results, a mesh of 3 mm is chosen. Furthermore, no lumped mass is attached to the tape spring since the dynamic deployment is not analysed yet. As opposed to the conditions described in Section 4, both the folding and the unfolding are then quasi-static so the Newmark method is used in both phases.

The impact of two geometric parameters is analysed: the thickness t and the radius of curvature R. Regarding the latter, in order to compare similar models, the width of the tape spring is kept constant and the subtended angle α is then modified accordingly.

5.1 Influence of the thickness

The influence of the thickness on the evolution of the bending moment when the folding and unfolding of the tape spring are quasi-static is summarised in Fig. 6, where only four curves are represented and the abscissa axis spans from $-15°$ to 15° for the sake of visibility. Since the thickness is the only variable, the radius of curvature R is fixed to 20 mm and the subtended angle α to 90°. The full lines correspond to the loading sequence, while the dashed lines correspond to the controlled unloading of the tape spring.

For each value of the thickness, the overall evolution in the opposite sense respects the theoretical description given in Section 3: at first, the bending moment increases linearly, then it reaches a maximum followed by a sharp drop due to buckling and finally a quasi-constant steady-state moment is obtained; in the unloading part, the fold disappears for a bending angle

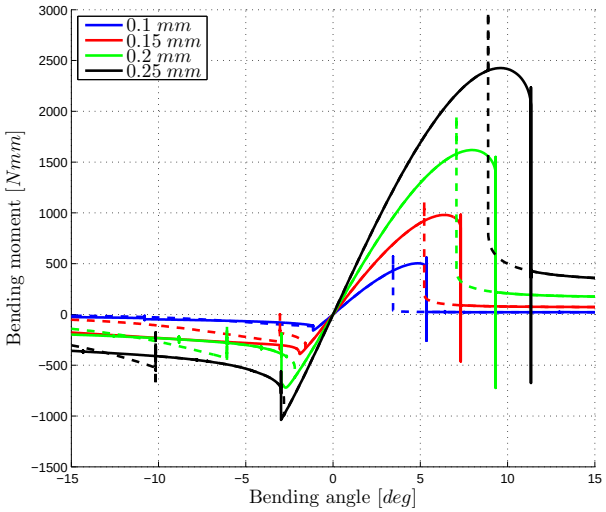

Figure 6: Influence of the thickness on the evolution of the bending moment with respect to the bending angle in opposite and equal senses (full lines = loading, dashed lines = unloading).

smaller than the one associated to buckling. The only discrepancies are the vertical peaks visible at these two angles. They are purely numerical and are due to the transient behaviour of the Newmark solver.

The evolution in equal sense bending requires more explanations. During the folding, a first large peak is encountered. In terms of deformation, it corresponds to the formation of torsional folds. Then, for higher bending angles, these folds move towards the middle of the tape springs. Due to the meshing, these displacements are not perfectly smooth and can create vertical peaks around the curves. These latter are numerical and can be avoided by refining the mesh as it was discussed in [11]. Then, the torsional folds combine themselves to form a symmetric one which is noticeable on the curve by the last jump before finally reaching the quasi-constant steady-state moment. During unloading, a similar procedure is followed in the reverse order: the symmetric fold divides itself into torsional folds, then these latter move away from each other to finally disappear as the bending angle is reduced. However, in this case, the division of the symmetric fold is responsible for a larger peak. Furthermore, the associated bending angles are not necessarily the same as those characterising the loading. All these elements lead to the non-superposition of the loading and unloading paths. The equal sense bending behaviour obtained through finite element analyses is then more complex than what is commonly accepted in theory.

As can be expected, structures with a larger thickness are stiffer. In Fig. 6, this behaviour is illustrated by the larger slopes at the origin which lead to higher peak moments in both senses. Accordingly, the phenomenon of buckling is triggered for higher absolute bending angles.

When comparing the areas subtended by the loading and unloading curves in opposite sense, larger differences are visible for stiffer tape springs. It implies that the dissipation of energy by hysteresis has a stronger impact on the behaviour of the structure as the thickness increases (Fig. 7). As the vibration frequency also increases with the thickness, it can then be expected that, after deployment, the oscillations of a thick tape spring require a shorter period of time to be damped out. In equal sense, the evolution of the dissipated energy is less smooth due to the numerical peaks that disturb the loading and unloading paths before and after buckling as discussed previously. Indeed, it is clearly visible that for a thickness of 0.15 mm, the amount of energy dissipated by hysteresis is overestimated. Nonetheless, the

overall increase of the other results is preserved. Finally, without taking into account the obvious overestimation, more energy is dissipated in opposite sense than in equal sense.

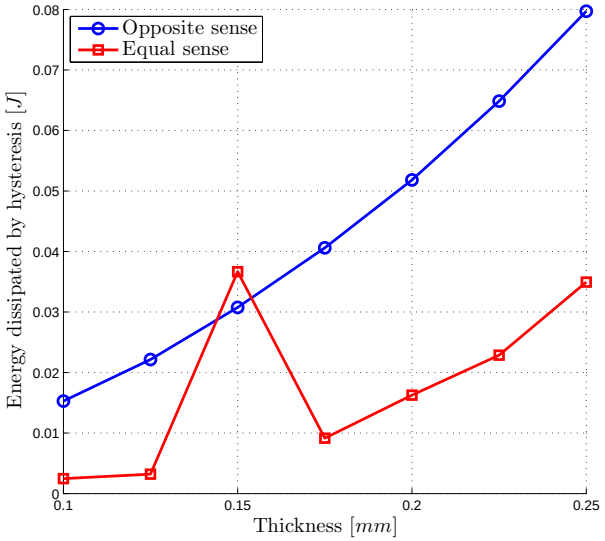

Figure 7: Influence of the thickness on the amount of energy dissipated by hysteresis.

The last critical parameter that will affect the choice of the tape spring geometry is the maximum Von Mises stresses reached in the structure throughout its folding and deployment. In the case of these quasi-static analyses, the results in opposite and equal senses are given in Fig. 8 where it can be seen that the stresses increase almost linearly with the thickness. In practical applications, it is then necessary to fix an upper limit to this geometric parameter in order to keep the deformations in the elastic regime. Indeed, with a thickness of 0.25 mm, a quasi-static loading already leads to stresses higher than the yield limit of the beryllium copper (Table 1) in opposite sense, while in equal sense, the threshold is exceeded for a thickness of less than 0.2 mm.

5.2 Influence of the radius of curvature

In order to understand the influence of the radius of curvature R on the behaviour of a tape spring, similar models must be compared. In order to do so, the width, that is the chord joining the extremities of the tape spring cross-section, is fixed to the value used in the previous section. It implies then that the subtended angle α has to be modified in accordance with the radius of curvature R. Furthermore, only a specific interval of radii can be studied in order to keep geometries representative of tape springs. Indeed, if the subtended angle exceeds 180°, the structure becomes tubular and some contacts on the internal surface occur during folding. Extensive analyses of tubular compliant hinges can be found in [26, 27]. On the other hand, if the radius of curvature is too high and accordingly the subtended angle too small, all the attractive properties in terms of dissipation, self-locking and self-actuation in tape springs are lost, since the structure tends to behave as a flat plate. Finally, to fully define the models, the thickness is set to 0.1 mm and the material is still the beryllium copper, the properties of which are given in Table 1.

The evolution of the bending moment for four different radii of curvature is given in Fig. 9, where the interval of the bending angle spans from $-10°$ to $10°$ for the sake of clarity. As it was the case in Fig. 6, the full lines represent the loading sequence, while the dashed ones represent

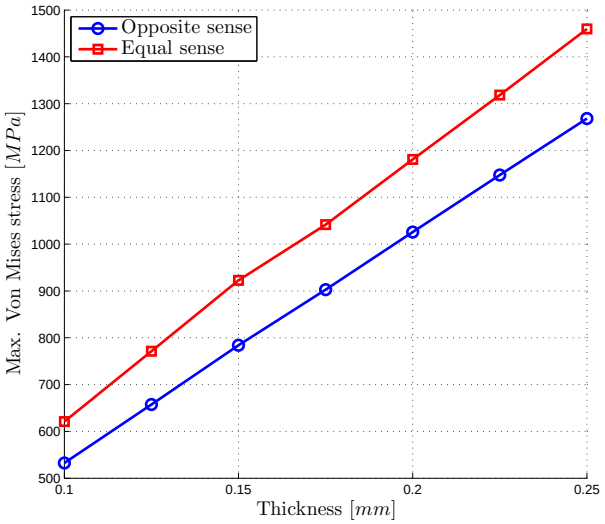

Figure 8: Influence of the thickness on the maximum Von Mises stresses.

the controlled unloading. In both senses, the expected behaviour is recovered, with again a more complex evolution in equal sense than the one described in theory (Section 3) and slightly disturbed by the same numerical phenomena as described in the previous section.

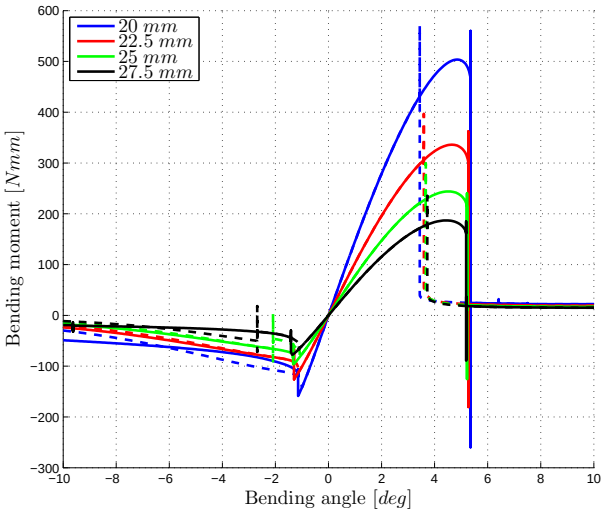

Figure 9: Influence of the radius of curvature on the evolution of the bending moment with respect to the bending angle in opposite and equal senses (full lines = loading, dashed lines = unloading).

Increasing the radius of curvature leads to the diminution of the absolute value of the peak moments in both senses. Indeed, since the tape spring becomes flatter, its stiffness decreases and the required moment to bend it is naturally reduced. However, unlike the previous parametric study, the associated bending angles do not vary significantly: for example in opposite sense, a decrease of only 10.2 % is noticed between the two extreme analysed cases, while an increase of 160 % is reached when only the thickness varies. Regarding the steady-state moments reached

after the formation of the fold, stiffer tape springs are logically characterised by larger moments, however, as for the bending angles, a change of radius does not lead to a large variation of the steady-state moments.

Focusing on the opposite sense bending, since the bending angles corresponding to buckling and the disappearance of the fold are very similar for each model, the highest dissipation by hysteresis is encountered in the tape spring with the smallest radius of curvature (Fig. 10). It can then be expected that the oscillations resulting from the deployment stage are damped out in a shorter period of time. On the other hand, as mentioned in the previous section, the behaviour in equal sense bending is intrinsically more complex and does not allow an evolution as clear as in the opposite sense, but the general decrease is preserved. Furthermore, as it was also the case in the previous section, the dissipation by hysteresis is more significant in opposite sense than in equal sense.

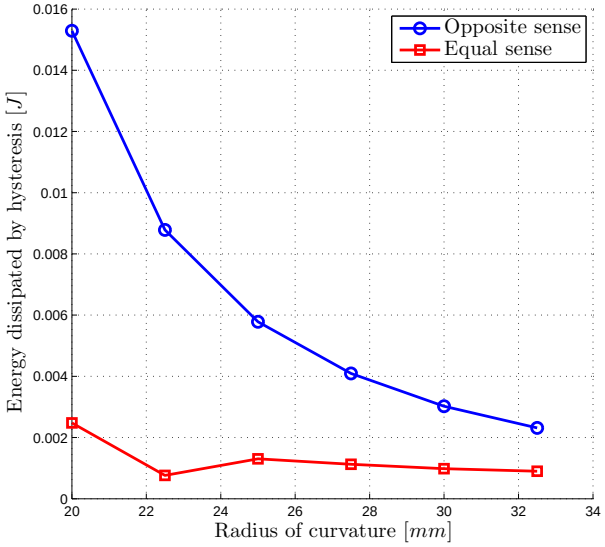

Figure 10: Influence of the radius of curvature on the amount of energy dissipated by hysteresis.

Finally, compared to the thickness (Fig. 8), the radius of curvature has the opposite effect on the evolution of the maximum Von Mises stresses. Indeed, increasing this parameter leads to a less stiff tape spring and logically the stresses are reduced when it is deformed (Fig. 11). In terms of values, the maximum Von Mises stress reached in equal sense is at least 16.9 % higher than in opposite sense.

6 Optimisation on a single tape spring

In order to determine the most efficient tape springs which meet the requirements for the deployment of the reflector defined in Section 2, an optimisation procedure is proposed. As mentioned previously, only the thickness t, the radius of curvature R and the subtended angle α are chosen as design variables, while the length L and the material properties are fixed to 50 mm and beryllium copper respectively.

The selection of the geometric parameters is first performed on a single tape spring connected to a lumped mass representing half of the reflector inertia, both in opposite and equal senses. Nonetheless, as mentioned in Section 2, the final hinge in this practical application is composed of two tape springs in order to restrain the lateral displacements due to torsion and

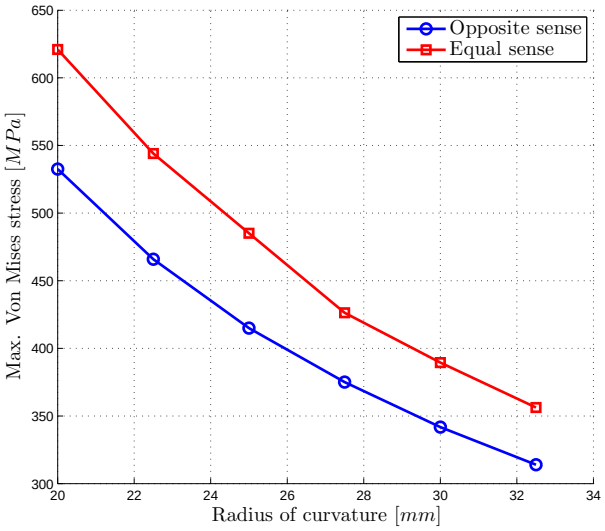

Figure 11: Influence of the radius of curvature on the maximum Von Mises stresses.

guide the deployment motion. Since limited torsional and three-dimensional behaviours could be expected, the results obtained for one tape spring have then to be confirmed for the complete hinge *a posteriori*.

6.1 Optimisation procedure

The optimisation procedure exploits the active set algorithm available in the MATLAB software through the *fmincon* function which solves constrained nonlinear multivariable problems of medium scale [28]. The optimisation problem to be solved can be expressed as:

$$\min_x f(x) \text{ such that } \begin{cases} c(x) \leq 0 \\ lb \leq x \leq ub \end{cases} \tag{1}$$

where $f(x)$ is the objective function to be minimised with respect to the vector of design variables x, $c(x)$ contains the nonlinear inequality constraints, and lb and ub are the vectors containing respectively the lower and upper bounds of the design variables. A termination tolerance of 10^{-3} is chosen on the variation of the objective function and the design variables, while the tolerance on the constraints violation is also set to 10^{-3}. Notice that the optimisation function *fmincon* only determines local minima. The initial guess of the design parameters has then an impact on the solution and has to be chosen with care by the designer.

The nonlinear inequality constraints are the two limits imposed on the width and the height of the tape spring cross-section. They are expressed as the following trigonometric functions:

$$\begin{cases} c_1(\alpha, R) &= 2R \sin \frac{\alpha}{2} - w_{\max} &\leq 0 \\ c_2(\alpha, R) &= R\left(1 - \cos \frac{\alpha}{2}\right) - h_{\max} &\leq 0 \end{cases} \tag{2}$$

with $w_{\max} = 25\ mm$ and $h_{\max} = 10\ mm$ as it was decided in Section 2.

Regarding the lower and upper bounds of the design variables, they are defined in Table 2 based on our experience acquired during the parametric studies such that even in the extreme cases, the tape spring still preserves its advantageous features.

The optimisation procedure is as follows. Starting from an initial geometry, the design variables are introduced in the SAMCEF software which creates the corresponding finite element

	$t\ [mm]$	$R\ [mm]$	$\alpha\ [deg]$
lb	0.08	10	60
ub	0.25	32.5	135

Table 2: Lower and upper bounds of the design variables.

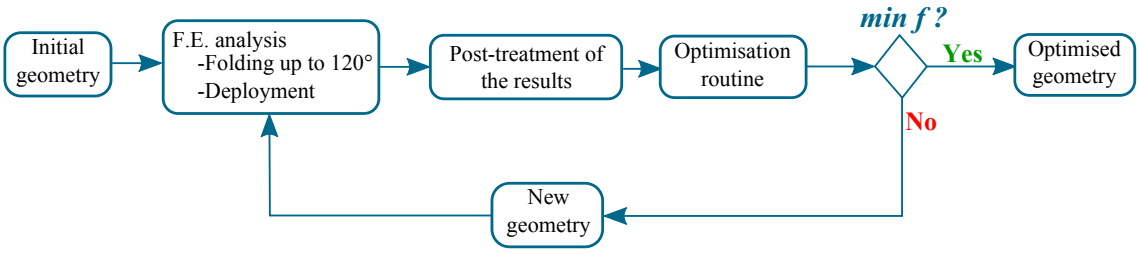

Figure 12: Optimisation procedure.

model and then solves it. The results are post-treated in order to extract the value of the objective function and the nonlinear equality constraints. They are then sent back to the optimisation routine in MATLAB which checks the validity of the constraints and the minimisation of $f(x)$. If these two conditions are respected, the optimised geometry is found, otherwise, the optimisation routine determines automatically the next configuration to be analysed and a new cycle is carried out. This procedure is schematically represented in Fig. 12.

In the SAMCEF software, each analysis follows the same pattern. First, the structure is folded until the bending angle reaches 120°. In order to keep a quasi-static evolution, this step is performed in 240 s during which the time is directly related to the bending angle by a coefficient of 0.5. Then, the tape spring is deployed and its behaviour is studied for 30 s. Regarding the boundary conditions, the tape spring is clamped at one extremity, while the transverse displacements are locked along its median, since as mentioned previously, for the complete system, these displacements and hence the torsion in equal sense bending should be limited.

This procedure is performed for the two senses of bending (opposite and equal) since each one is characterised by a distinct behaviour and a specific deformed configuration. Furthermore, it implies that for the complete system composed of two tape springs, three configurations are possible: both tape springs initially folded at an angle of 120° in opposite sense, both tape springs initially folded in equal sense and the alternate configuration in which both senses of bending are present. The orientation of the tape springs is then also a design variable, but the choice is performed after the optimisation procedure summarised in Fig. 12. Finally, for symmetry reasons, both tape springs will have the same optimised geometry.

6.2 Minimisation of the maximum Von Mises stress

In this first case, the optimisation procedure aims at minimising the maximum Von Mises stress $\sigma_{\max}$ reached in the whole tape spring during folding and deployment, while the maximum motion amplitude $\beta_{\max}$ is left free of constraints. It means then that in the expression of the problem Eq. (1), the objective function is defined as $f(x) = \sigma_{\max}$.

The results of the optimised procedure are given in Table 3, along with the initial geometry. Notice that for this latter, the thickness is already set to its lowest bound, since, as it was shown in Fig. 8, increasing this parameter only leads to higher values of the maximum Von Mises stress.

Starting from the same geometry, the optimised results are different according to the

	t $[mm]$	R $[mm]$	α $[deg]$	$\sigma_{\max}$ $[MPa]$	$\lvert\beta_{\max}\rvert$ $[deg]$	Nbr. of func. eval.
Initial geometry	0.08	17.5	90	–	–	–
Opt. geometry (opposite sense)	0.08	10	60	**861.68**	205.95	8
Opt. geometry (equal sense)	0.08	15.79	60	**647.33**	57.05	61

Table 3: Results for the minimisation of the maximum Von Mises stress $\sigma_{\max}$.

sense of bending in terms of the radius of curvature R, this latter being larger in equal sense, while it is set to the lowest bound in opposite sense. Regarding the subtended angle α, the lowest bound is also the optimised value and as expected, the smallest allowed thickness t is retained. Finally, it can be seen that the optimised geometry in opposite sense was obtained after 8 function evaluations, that is that 8 different models were solved before reaching the one described in Table 3, while 61 function evaluations were performed in equal sense.

Regarding the objective function, the maximum Von Mises stresses $\sigma_{\max}$ for the optimised geometries are, as required, below the yield limit in both senses in order to keep the deformations in the elastic regime. Nonetheless, larger stresses are encountered in opposite sense. Indeed, the maximum value is 33.11 % higher than in equal sense.

The last extracted results are linked to the maximum motion amplitude $\beta_{\max}$, which in this case is not part of the objective function. First of all, the displacements at the extremity of the tape spring are given in Fig. 13 for the two types of initial foldings and focus on the deployment stage. It can be seen that despite starting from almost the same point at 240 s (the small discrepancies being due to the different deformed configurations as illustrated in Fig. 4), the motion amplitude is much smaller in equal sense. However, even after 30 s, the tape spring keeps oscillating in both cases. This design is then not efficient in a space environment where a weak motion damping yields a long waiting period before the stabilisation of the spacecraft and hence the use of precise instruments. In the next section, it will be shown that minimising the motion amplitude greatly helps solving this problem.

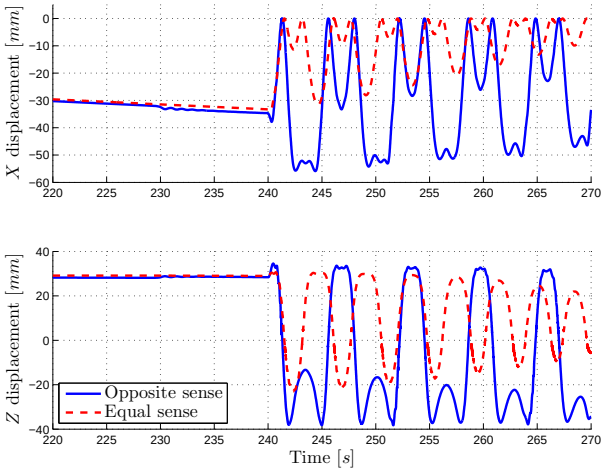

Figure 13: Evolution of the displacements at the extremity of the tape spring in both senses in the case $f(x) = \sigma_{\max}$.

To quantify the motion amplitude, Figs. 14 and 15 which show the complete deployment of the reflector and the tape spring in the xz-plane are used. In both figures, the straight green

line represents the non-deformed tape spring, the straight black line represents the deployed reflector and the straight blue line represents the fixed solar panel. The orientation of the frame is as defined in Section 2, that is aligned on the non-deformed tape spring. The quasi-circular arcs show the position of the tape spring extremity and of the lumped mass (located at the reflector centre of mass) during the different time steps of the dynamic analysis. Finally, the red squares correspond to the position of the reflector when the tape spring is folded up to an angle of 120°, the reflector is then parallel to the solar panel; and the red circles correspond to the position of the reflector in the most extreme configuration reached in the transient phase. The maximum motion amplitude $\beta_{\max}$ is then defined as the maximum angle between this last line and the reflector in its deployed configuration (straight black line). The complete evolution of the angle β is given in Fig. 16 where the fully folded configuration corresponds to $\beta = 120°$ and the stabilised deployed configuration corresponds to $\beta = 0°$ (not reached here due to the slow damping of the oscillations). The sign of this angle is defined as positive in the first and second quadrants if the extremity of the reflector is above the solar panel and as negative in the second quadrant if the extremity of the reflector is below the solar panel, as well as in the third and forth quadrants.

The summary of the results on the deployment obtained after minimising the maximum Von Mises stress are given in Table 3. It can be clearly seen, both numerically and visually, that, as predicted by Figs. 13 and 14, the larger motion amplitude is encountered when the tape spring is initially folded in opposite sense. Nonetheless, no collision occurs with the solar panel.

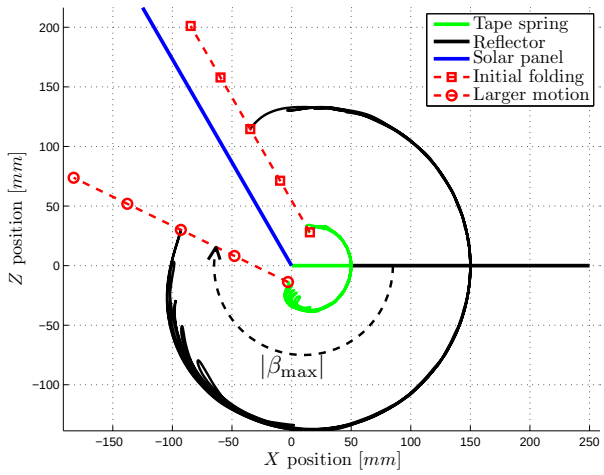

Figure 14: Deployment of the tape spring in opposite sense in the case $f(x) = \sigma_{\max}$.

6.3 Minimisation of the maximum motion amplitude

In this second case, the aim is to minimise the maximum motion amplitude $\beta_{\max}$, while the maximum Von Mises stress $\sigma_{\max}$ is left free to vary. The objective function in Eq. (1) is then defined as $f(x) = \beta_{\max}$.

The optimised results are obtained in opposite and equal senses after 38 and 57 function evaluations respectively. Notice that two different initial geometries have to be used to reach the minimum motion amplitude since, as exposed in Section 6.1, the optimisation function determines only local minima. The geometric characteristics are given in Table 4 where it can be seen that the optimised tape springs are similar in both senses, the thickness t and the radius

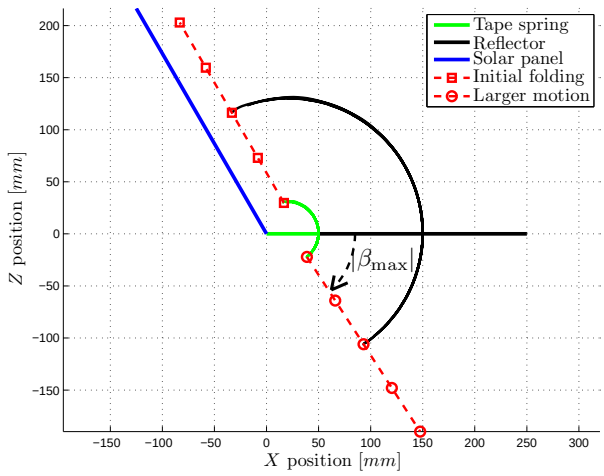

Figure 15: Deployment of the tape spring in equal sense in the case $f(x) = \sigma_{\max}$.

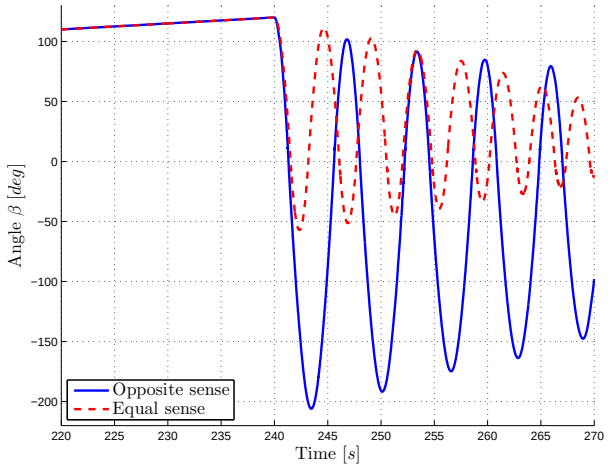

Figure 16: Evolution of the angle β in both senses in the case $f(x) = \sigma_{\max}$.

of curvature R being equal or close to their lowest limit, while a large subtended angle α is required.

The maximum motion amplitude $\beta_{\max}$ is obviously reduced compared to the results obtained after solely minimising the maximum Von Mises stress as it can be seen quantitatively in Table 4 and qualitatively in Figs. 17 and 18, which illustrate the deployment sequence in the xz-plane for an initial folding in opposite and equal sense respectively. These figures also confirm the absence of collision between the reflector and the solar panel.

The evolution of the displacements at the extremity of the tape spring are given in Fig. 19 where the abscissa axis spans from 220 s to 250 s. As could be expected, minimising the maximum motion amplitude leads to smaller displacements after deployment. Regarding the oscillations, they are characterised by a higher frequency and they are quickly damped out after ~ 6 s in opposite and equal senses, while previously 30 s were not nearly enough. Obviously, this behaviour is also apparent in the evolution of the angle β with respect to time (Fig. 20).

However, minimising the maximum motion amplitude comes at the expense of the Von

	t $[mm]$	R $[mm]$	α $[deg]$	$\sigma_{\max}$ $[MPa]$	$\lvert\beta_{\max}\rvert$ $[deg]$	Nbr. of func. eval.
Initial geometry (opposite sense)	0.08	10	131	–	–	–
Opt. geometry (opposite sense)	0.08	10.03	130.72	2545.7	**114.71**	38
Initial geometry (equal sense)	0.25	10	135	–	–	–
Opt. geometry (equal sense)	0.0846	10.11	124.10	1448.7	**6.17**	57

Table 4: Results for the minimisation of the maximum motion amplitude $\beta_{\max}$.

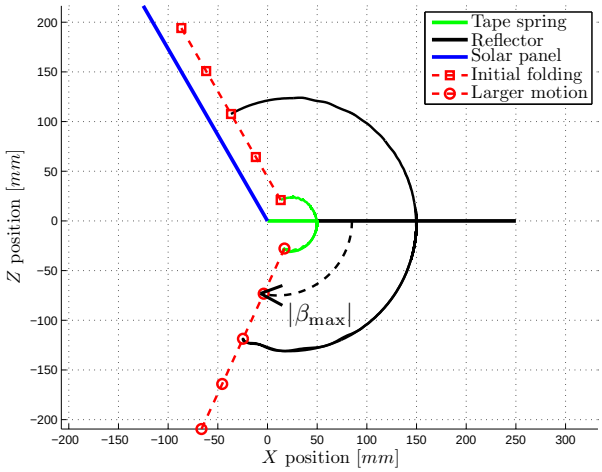

Figure 17: Deployment of the tape spring in opposite sense in the case $f(x) = \beta_{\max}$.

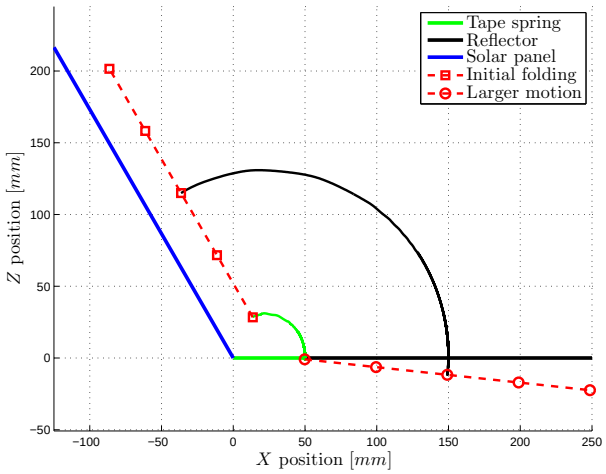

Figure 18: Deployment of the tape spring in equal sense in the case $f(x) = \beta_{\max}$.

Mises stresses for which the maximum clearly exceeds the yield limit of the beryllium copper, whatever the initial sense of folding (Table 4). The deformations are then such that, after deployment, a straight configuration might not be recovered due to irreversible damage of the tape spring. Notice that in this work, the finite element models do not take plastic deformations into account.

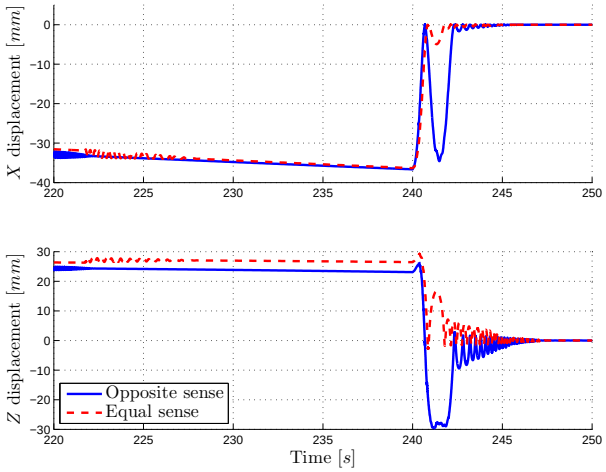

Figure 19: Evolution of the displacements at the extremity of the tape spring in both senses in the case $f(x) = \beta_{\max}$.

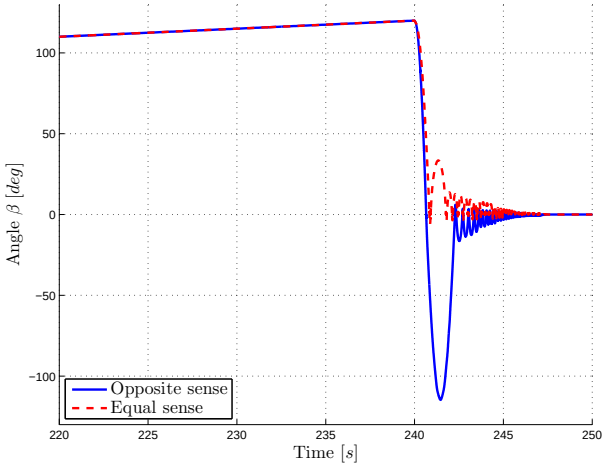

Figure 20: Evolution of the angle β in both senses in the case $f(x) = \beta_{\max}$.

6.4 Minimisation of a weighted objective function

In this third case, the objective function is a combination of the two previous problems. It is then defined as a weighted sum of the maximum Von Mises stress $\sigma_{\max}$ and the maximum motion amplitude $\beta_{\max}$ such that:

$$f(x) = w_1\sigma_{\max} + w_2|\beta_{\max}| \tag{3}$$

where w_1 and w_2 are weights respectively expressed in deg and MPa. In this optimisation procedure, the choice is made to use $w_1 = 0.1w_2$ in order to sum two terms with a similar order of magnitude. Notice that the previous objective functions can be recovered by setting alternatively the weights to zero.

The results are given in Table 5 along with the number of function evaluations required to reach them. Starting from the same model, the optimised geometry is the same for the two different folding senses. For an initial folding in equal sense, it corresponds to a tape

	t $[mm]$	R $[mm]$	α $[deg]$	$\sigma_{\max}$ $[MPa]$	$\lvert\beta_{\max}\rvert$ $[deg]$	Nbr. of func. eval.
Initial geometry	0.2	20	60	–	–	–
Optimised geometry (opposite sense)	0.08	10	60	**861.68**	**205.95**	23
Optimised geometry (equal sense)	0.08	10	60	**824.34**	**39.67**	30

Table 5: Results for the minimisation of the weighted objective function.

spring which achieves a compromise between the performances obtained by minimising the two objective functions separately. However, in opposite sense, the geometry minimising the maximum Von Mises stress $\sigma_{\max}$ is recovered.

Quantitatively, a larger maximum Von Mises stress is reached in opposite sense whereas it was shown in the parametric studies that folding a tape spring in equal sense leads to larger stresses. However, the values given in Table 5 are the maximum of both the quasi-static folding and the dynamic deployment. In this case, the maxima are reached right after triggering the deployment and the amount of potential energy inside a tape spring folded up to an angle of 120° in opposite sense is almost twice the amount in equal sense. It explains then that larger stresses are encountered after deploying a tape spring initially bended in opposite sense.

Regarding the evolutions of the displacements at the extremity of the tape spring and of the angle β (Figs. 21 and 22), the results are also between the two previous extreme cases in equal sense, both in terms of frequency of oscillations and time of damping, while in opposite sense the curves are the same as the one presented in Figs. 13 and 16 respectively. It implies then that it is characterised by the same drawback in terms of damping time.

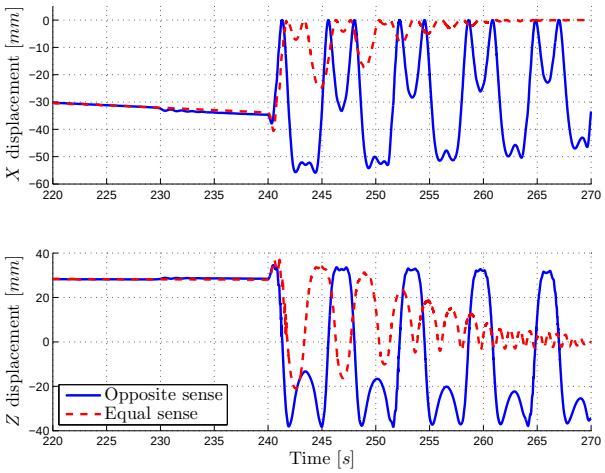

Figure 21: Evolution of the displacements at the extremity of the tape spring in both senses in the case Eq. (3).

Thus, these last analyses lead to two tape springs which stay in the elastic regime throughout the folding and the deployment sequence, and avoid any collision between the reflector and the solar panel. However, the structure starting with a fold in equal sense is stabilised in a much shorter period of time than the case in opposite sense.

The objective function defined by a weighted sum and used in this section is a pragmatic approach to minimise several parameters at the same time. However, its results are directly influenced by the selected values of the weights w_1 and w_2. An alternative approach is to deter-

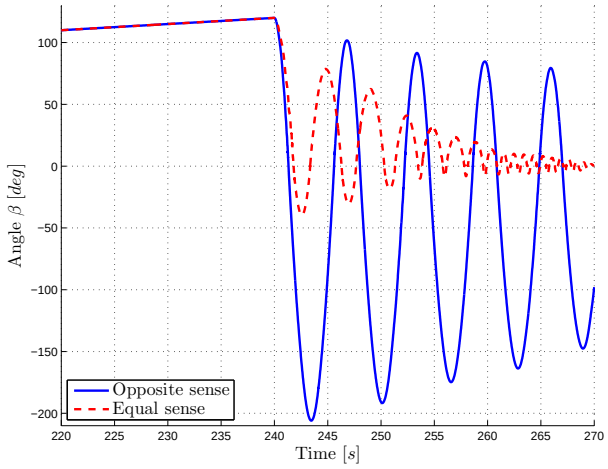

Figure 22: Evolution of the angle β in both senses in the case Eq. (3).

mine the Pareto front of the multi-objective optimisation problem. The Pareto front represents all the possible compromises which minimise the multi-objective function while respecting the constraints. For each point on the Pareto front, it is not possible to improve one of the objective functions without degrading the result of the others (*e.g.*, in this case it is not possible to reduce to value of the maximum Von Mises stress $\sigma_{\max}$ without increasing the value of the maximum motion amplitude $\beta_{\max}$, and vice versa).

A number of points of the Pareto front for both senses of folding have been computed and are given in Fig. 23 where all the optimised results summarised in Tables 3, 4 and 5 can easily be recovered. In the remaining parts of this work, the results given in Table 5 will be exploited as it represents a fair compromise between the maximum Von Mises stress $\sigma_{\max}$ and the maximum motion amplitude $\beta_{\max}$. Furthermore, the optimised geometry is conveniently the same in both senses of folding.

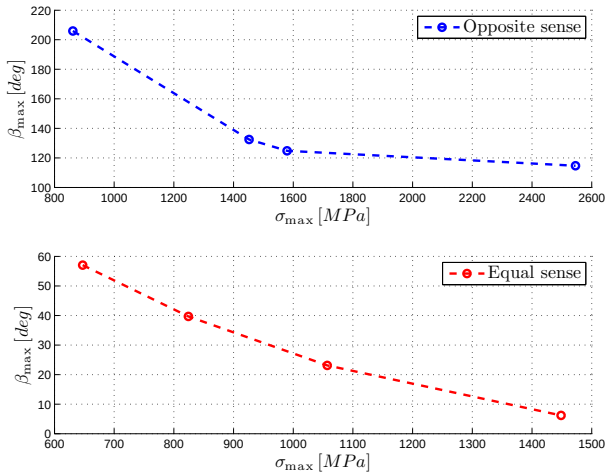

Figure 23: Pareto front in opposite and equal sense for a multi-objective function on $\sigma_{\max}$ and $\beta_{\max}$.

7 Deployment of the reflector

The optimised geometry obtained in the previous section with the weighted sum is now exploited to define the tape springs composing the hinge described in Section 2. A schematic illustration of the finite element model is given in Fig. 24. Regarding the boundary conditions, as mentioned previously, the solar panel is considered as already deployed and fixed, the tape springs are then clamped at these extremities and the transverse displacements are not constrained since they should be limited thanks to the configuration of the hinge. The reflector is represented as a lumped mass (red dot) located at its centre of mass and rigidly connected to the extremities of the tape springs. Finally, the gap between these latter is chosen as large as possible while keeping a margin of 5 mm on each lateral sides of the reflector.

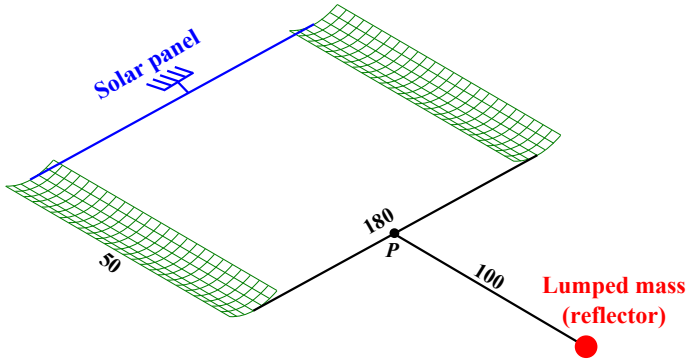

Figure 24: Illustration of the finite element model of the hinge (dimensions in millimetres, not to scale).

As it was proven an a single tape spring, an initial folding in equal sense leads to smaller values of maximum Von Mises stress $\sigma_{\max}$ and maximum motion amplitude $\beta_{\max}$ compared to an initial folding in opposite sense. Furthermore, the amount of time required to damp out the oscillations of the motion is also reduced. The solution of the problem stated in Section 2 is then to perform the deployment of the reflector with the hinge initially bended in equal sense.

The evolution of the angle β between the fully deployed configuration of the reflector and its transient position during the deployment is given in Fig. 25 where the results for a hinge initially folded in opposite sense and the alternate configuration (one tape spring folded in opposite sense and the other one folded in equal sense) are also shown for the sake of completeness. As expected, a hinge only folded in equal sense has a smaller motion amplitude and is more quickly stabilised than the two other configurations.

Furthermore, the maximum Von Mises stress $\sigma_{\max}$, the maximum motion amplitude $|\beta_{\max}|$ and the maximum lateral displacement $|Y_{\max}|$ are given in Table 6, where Eq.-Eq. (resp. Opp.-Opp.) is the case with the two tape springs initially folded in equal sense (resp. opposite sense) and Opp.-Eq. is the alternate configuration. The differences compared to Table 5 are due to the fact that the lateral displacements of the tape spring medians are now left free of constraints while previously they were fixed to zero. Nonetheless, in the case Eq.-Eq., the results have not varied much. Regarding the lateral displacements, as expected, they remain small proving thus that the two tape springs configuration restrains the effects of the torsion and it confirms our choice of boundary conditions in the optimisation procedure on a single tape spring. Finally, for the alternate configuration Opp.-Eq., the maximum values are logically between the two other cases.

To conclude these last results, the optimised geometry for the tape springs of the hinge leads to a deployment avoiding any collision with the solar panel and stresses such that the

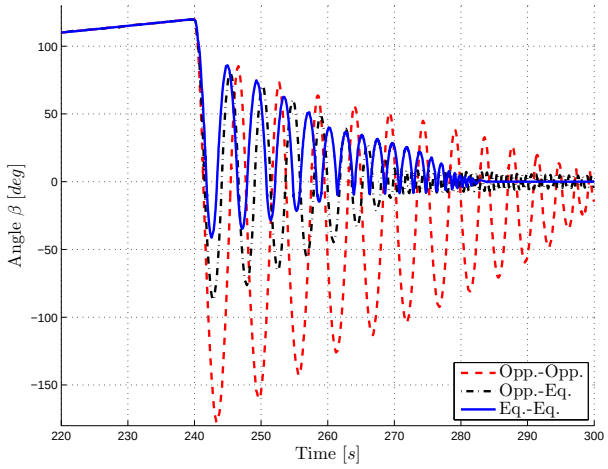

Figure 25: Evolution of the angle β for the hinge at point P.

	Eq.-Eq.	Opp.-Eq.	Opp.-Opp.
$\sigma_{\max}$ $[MPa]$	827.78	895.61	908.26
$\lvert\beta_{\max}\rvert$ $[deg]$	41.29	87.21	177.75
$\lvert Y_{\max}\rvert$ $[mm]$	0.44	0.83	0.35

Table 6: Maximum values for the three configurations of the tape springs in the hinge.

deformations stay in the elastic regime. The reflector can then be safely deployed.

8 Conclusions

In this paper, an optimisation procedure is developed in order to determine the geometry of tape springs. The intended purpose is, in the end, to use a hinge composed of two of these tape springs to deploy a reflector around a solar panel. These mechanisms are chosen due to their passive behaviour, their self-locking capacity, their elastic deformations and their robustness. The progress of this work follows three main steps.

First of all, the impact of the geometry on the tape spring nonlinear behaviour is studied by the means of quasi-static parametric analyses which imply the folding and the controlled deployment of the structure at a rate of 0.5° per second. It is shown that for a chosen width, a small thickness and a large radius of curvature lead to low Von Mises stresses and only a small amount of energy is dissipated by hysteresis whatever the sense of bending. Nonetheless, the two bending senses are not characterised by the same values, the phenomenon of hysteresis being more pronounced in opposite sense, while larger Von Mises stresses are encountered in equal sense.

Then, the optimisation procedure is defined on a single tape spring. The design variables are the thickness, the radius of curvature and the subtended angle of the tape spring, the length and the material characteristics being fixed *a priori*. Two types of constraints are enforced: nonlinear constraints which limit the maximum width and height of the tape spring cross-section, and lower and upper bounds directly limiting the value of the design variables. The optimised geometry is determined for three objective functions to be minimised: the maximum Von Mises stress, the maximum motion amplitude and a weighted sum of these two functions.

At the end of the optimisation procedure, a tape spring that remains in the elastic regime throughout the folding and the deployment, and has a motion that does not collide with the solar panel is obtained. It is found that an initial folding in equal sense presents the best characteristics.

Finally for the last step, this optimised geometry is used to form the complete hinge composed of two tape springs. The finite element simulation shows the absence of plastic deformation and collision. Furthermore, the lateral displacements and hence the torsion is restrained. This work shows thus that a reflector could be deployed by the means of tape springs and that the careful choice of the geometry and the orientation lead to various deployment behaviours.

Acknowledgements

The first author would like to acknowledge the Belgian National Fund for Scientific Research for its financial support.

References

References

[1] S. Pellegrino, Deployable structures in engineering, *Deployable Structures*, CISM Courses and Lectures, vol. 412, Springer (Wien), 2001.

[2] W. Wüst, Einige Anwendungen des Theorie der Zylinderschale, *Z. Angew. Math. Mech.* **34**, 1954, 444–454.

[3] F.P.J. Rimrott, Querschnittsverformung bei Torsion offener Profile, *Z. Angew. Math. Mech.* **50**, 1970, 775–778.

[4] E.H. Mansfield, Large-deflexion torsion and flexure of initially curved strips, *Proc. R. Soc. Lond.* **A 334**, 1973, 1125–1132.

[5] K.A. Seffen, S. Pellegrino, Deployment dynamics of tape-springs, *Proc. R. Soc. Lond.* **A 455**, 1999, 1003–1048.

[6] K.A. Seffen, On the behaviour of folded tape-springs, *ASME J. Appl. Mech.* **68**, 2001, 369–375.

[7] F. Guinot, S. Bourgeois, B. Cochelin, L. Blanchard, A planar rod model with flexible thin-walled cross-sections. Application to the folding of tape springs, *Int. J. Solids Struct.* **49 (1)**, 2012, 73–86.

[8] E. Picault, P. Marone-Hitz, S. Bourgeois, B. Cochelin, F. Guinot, A planar rod model with flexible cross-section for the folding and the dynamic deployment of tape springs: Improvements and comparisons with experiments, *Int. J. Solids Struct.* **51 (18)**, 2014, 3226–3238.

[9] K.A. Seffen, S. Pellegrino, Deployment of a rigid panel by tape-springs, *Department of Engineering, University of Cambridge, Report CUED/D-STRUCT/TR168.*, 1997.

[10] S. Hoffait, O. Brüls, D. Granville, F. Cugnon, G. Kerschen, Dynamic analysis of the self-locking phenomenon in tape-spring hinges, *Acta Astronaut.* **66**, 2010, 1125–1132.

[11] F. Dewalque, P. Rochus, O. Brüls, Importance of structural damping in the dynamic analysis of compliant deployable structures, *Acta Astronaut.* **111**, 2015, 323–333.

[12] S.J.I. Walker, G. Aglietti, Study of the dynamics of three-dimensional tape spring folds, *AIAA J.* **42**, 2004, 850–856.

[13] S.J.I. Walker, G. Aglietti, Experimental investigation of tape springs folded in three dimensions, *AIAA J.* **44**, 2006, 151–159.

[14] K.A. Seffen, Z. You, S. Pellegrino, Folding and deployment of curved tape springs, *Int. J. Mech. Sci.* **42**, 2000, 2055–2073.

[15] K. Kwok, S. Pellegrino, Viscoelastic effects in tape-springs, in: *52nd AIAA/ASME/ASCE/ AHS/ASC Structures, Structural Dynamics and Materials Conference*, Denver, CO, 4-7 April 2011.

[16] I. Sokolsky, M.A. Brown, Naval Research Laboratory solar concentrator program, *AIP Conference Proceedings* **420**, 1998, 282–287.

[17] J.M. Bodeau, Root cause of the BSS 702 concentrator array anomaly, *Space Power Workshop*, 2003.

[18] H. Saito et al., Small satellite REIMEI for auroral observations, *Acta Astronaut.* **69**, 2011, 499–513.

[19] K. Steele, E. Linder, J. Renshall, High specific power solar concentrator array for low cost commercial satellite, in: *Proceedings of the 5th European Power Conference*, Tarragona, Spain, 1998.

[20] Ö. Soykasap, Analysis of tape spring hinges, *Int. J. Mech. Sci.* **49**, 2007, 853–860.

[21] C. Calladine, The theory of thin shell structures. *Proc. Inst. Mech. Eng., Part A: J. Power Energy* **202**, 1988, 141–149.

[22] K.A. Seffen, Analysis of structures deployed by tape-springs (Ph. D. thesis), Cambridge University, United-Kingdom, 1997.

[23] S.A. Samtech, SAMCEF User Manual, Version 8.4, 2013.

[24] N. Newmark, A method of computation for structural dynamics, *ASCE J. Eng. Mech. Div.* **85**, 1959, 67–94.

[25] J. Chung, G. Hulbert, A time integration algorithm for structural dynamics with improved numerical dissipation: the generalized-α method, *ASME J. Appl. Mech.* **60**, 1993, 371–375.

[26] H.M.Y.C. Mallikarachchi, S. Pellegrino, Simulation of quasi-static folding and deployment of ultra-thin composite structures, in: *49th AIAA/ASME/ASCE/AHS/ASC Structures, Structural Dynamics, and Material Conference*, Schaumburg, Illinois, April 2008.

[27] M. Mobrem, D. Adams, Deployment analysis of lenticular jointed antennas onboard the mars express spacecraft, *J. Spacecr. and Rockets* **46**, 2009, 394–402.

[28] The MathWorks, Matlab, 2009, Version 7.9.0 (R2009b).